

# Lubrication With Granular Flow: Continuum Theory, Particle Simulations, Comparison With Experiment

**W. Gregory Sawyer**

Department of Mechanical Engineering,  
University of Florida,  
Gainesville, FL 32611

**John A. Tichy**

Department of Mechanical Engineering,  
Aeronautical Engineering, and Mechanics,  
Rensselaer Polytechnic Institute,  
Troy, NY 12180

*Studies of particle flows have followed three parallel paths: (1) experiment, (2) analysis based on the assumption of a continuum, and (3) direct particle simulation. In this paper, we perform continuum and particle analyses and compare them to each other, and to previously reported experiments. Both the particle simulations and the continuum model over-predict the experimental normal load and shear force, however, the trends and orders-of-magnitude are in agreement. The modeling approaches are based on first principles, and do not rely on curve fitting to obtain effective properties of the mixture such as viscosity or conductivity. [DOI: 10.1115/1.1353178]*

## Introduction

Over recent years there has been increasing interest in the possible use of granular or powder mixtures as a means of applying solid lubrication. At temperatures greater than 500°C, conventional liquid lubricants cannot be applied and powder lubrication may be an attractive alternative. There are a number of other tribological applications in which particulate two-phase flow may play a role. The process of chemical-mechanical polishing (CMP), which is a subject of intense interest in electronics manufacturing to attain a high degree of planarity on silicon wafers, involves the thin film flow of a slurry of particles (Ali et al. [1] and Tichy et al. [2]). The process of debris analysis for bearing diagnostics requires knowledge of such flows, Cho and Tichy [3]. Particulate debris migration associated with lysis (an inflammatory bone reaction) in artificial joint prostheses is a cause of failure, Poggie et al. [4]. Our present study is concerned with the flow of non-deforming granules without a carrier fluid, and, thus, strictly speaking, would apply directly only to the powder lubrication case mentioned. However, this works study can form a basis for extensions to the true two-phase flow case.

In this paper, we compare results of both continuum modeling and particle dynamic calculations to our existing experimental results, Yu et al. [5] and Yu and Tichy [6]. Two modes operation are observed in the experimental shear cells. At low speeds, there are strong and long-lasting contact forces between the highly compacted beads and the surfaces. At some increased critical speed (in our apparatus at 100 s<sup>-1</sup>), the upper surface lifts off as the beads mean free path increases due to increased agitation. We call this a transition to granular collision lubrication. The former regime could be called granular contact lubrication. If granular contact lubrication exists in a bearing, the global friction forces are due to persistent rubbing interactions within the ensemble of particles. The normal forces are carried by elastic or plastic compression of the particles in contact. If collision lubrication exists, both normal and tangential forces are due to collisions of the highly energized beads with the loading surfaces. Most theoretical studies are concerned with the collision mode. However, intuitively, it seems that in many instances, solid lubricating action through sustained particle contacts (granular contact lubrication) is the more common mode to support the sliding surfaces.

Since 1988, many papers in the tribology literature have ap-

peared describing advances in high temperature powder lubrication, by Heshmat and colleagues (e.g., Heshmat [7,8]). Khonsari and co-authors, (e.g., Dai et al. [9] and McKeague and Khonsari [10]) have applied complex constitutive equations for mixtures. In the tribology literature, no distinction appears to be made between the two modes of lubrication. However from a rheology perspective, Campbell and Zhang [11] refer to the two domains as “quasi-static” and “rapid” flow. They go on to say “it is still far from clear just where lie the limits to the two flow regimes.” This continues to be an active area of research; recently Savage [12] has developed a theory, based on a continuum mechanics approach, for slow dense flows of cohesionless granular materials for two-dimensional flows.

## Background—Particle Simulations

The majority of numerical simulations of granular collision flows are event driven. This means that the particle velocities post-collision (one time step later) are functions of the particles' velocities and positions during the collision state (current time step). The event driven simulations typically calculate a normal and tangential velocity for the colliding particles. The normal velocities post-collision are calculated assuming a binary collision of rigid spheres or disks that conserves momentum. A coefficient of restitution that accounts for energy dissipation during the collision is typically included. The analytical treatments of tangential velocities in particle/particle and particle/wall collisions are complex and vary considerably. Our particular implementation is described in some detail below.

Campbell and Brennen [13] performed two-dimensional simulations of Couette flows of granular materials and compared these simulations to the experimental results of Bagnold [14] and Savage and Sayed [15]. These authors have also performed studies on inclined channel flows of granular materials and compared these results to their own inclined chute experiments. The computer simulations used inelastic circular cylinders, periodic boundaries perpendicular to the flow direction, an upper moving wall, a lower stationary wall, and a simulation length (distances separating the two periodic boundary walls) of 5 times the particle diameters. The authors ran these simulations until a steady state condition was obtained. In these studies, Campbell and Brennen used an event driven simulation with different coefficients of restitution for particle/particle and particle/wall collisions.

Walton and Braun [16] and Walton [17] have done a number of numerical studies in particulate two-phase flows, dry granular flows, and dry granular flows with non-spherical particles. In

Contributed by the Tribology Division for publication in the ASME JOURNAL OF TRIBOLOGY. Manuscript received by the Tribology Division October 21, 2000; revised manuscript received December 8, 2000. Associate Editor: M. M. Khonsari.

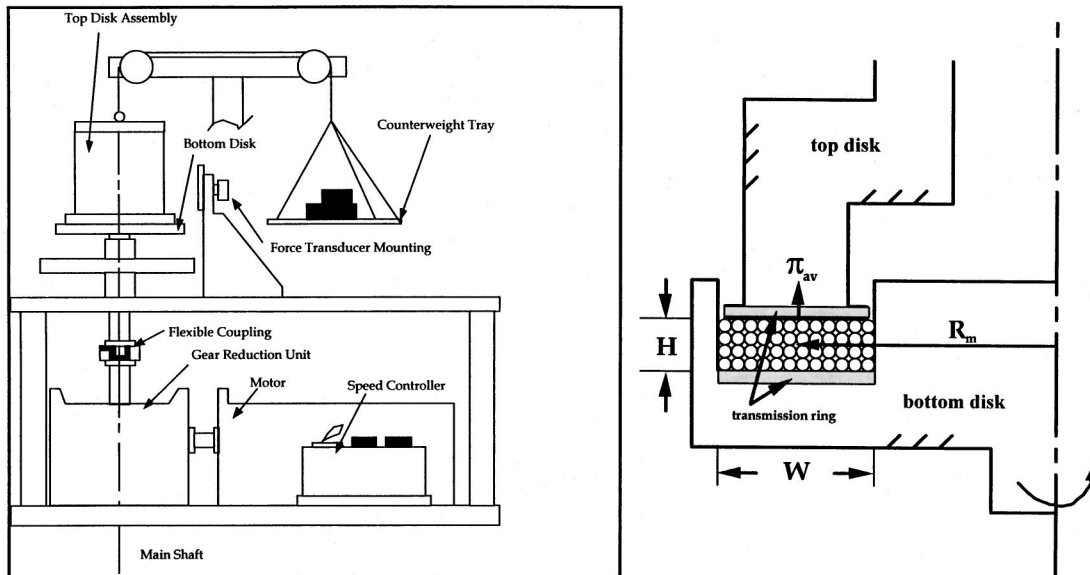


Fig. 1 Schematic of the shear cell apparatus

these studies they use both discrete element techniques and event driven, hard sphere, collision operators. Walton stresses the importance of using sufficiently realistic models for particle interactions. The author comments, "Eliminating such details as interparticle friction (and thus all particle rotation) may produce models that are simple and straight forward to evaluate; however, leaving out such important effects may produce a 'model material' that bears little resemblance to any real granular material." Their simulations are three dimensional with six degrees of freedom.

Campbell and Zhang [11] studied the phase-change behavior of dry granular flows in a three-dimensional discrete element simulation. The simulation was a Couette flow with periodic boundary conditions and 1000 particles. The periodic boundaries were spaced ten particle diameters across and the simulation geometry was approximately a cube (the film thickness was slightly greater than ten particle diameters). Although the authors included a friction coefficient ( $\mu=0.5$ ) and a coefficient of restitution ( $e=0.8$ ), the effect of these parameters on the flow behavior was not investigated.

Hopkins et al. [18] have investigated the structure of moderately dilute three-dimensional shear flows. A series of experiments were performed with 6859 spheres and a solid fraction  $v$  equaling 0.2. The simulation volume is a cube with no bounding surfaces; each face of the cube is a periodic boundary. The simulation is event driven, and the particles are modeled as frictionless spheres with a coefficient of restitution. The primary finding of this study is that a large particle system shows profound deviations from simple shear behavior that persist for considerable periods of time.

### Background—Experimental Study

The experimental shear cell apparatus is briefly described since it forms the reference point for the simulations. Using the experimental apparatus the effects of shear rate, packing fraction, particle size and film thickness on both the load carrying normal stress and the frictional shear stress can be investigated. The spheres are glass (average diameter  $D=0.787$  mm, density  $\rho_p=2550$  kg/m<sup>3</sup>), the height of the channel  $H$  is 4 mm, the channel is 19 mm wide and the length along a central circumferential path  $L$  is 0.479 m. Linear surface sliding speed  $U$  varies between 0.4 and 2.8 m/s. The mean solid volume fraction  $\bar{v}$  used is 0.595 (the

theoretical maximum volume fraction for identically sized spheres is  $v_0 \cong 0.65$ ), and the applied normal stresses  $P_y$  vary between 2.25 and 5.55 kPa.

At the beginning of an experiment, the lower transfer surfaces are set in place. The trough is filled with a predetermined volume of test particles, see Fig. 1. The upper stationary annular disk is lowered into the annulus with a predetermined applied normal stress, both the lower transfer surface and the sidewalls of the annular ring move. Shearing is initiated and a computer data acquisition system monitors the trough velocity, film thickness, supporting load, and frictional torque. From these measurements we can calculate (a) the average shear rate, (b) the average load carrying normal stress, (c) the average frictional shear stress, and (d) the solids volume fraction.

In these previous studies the effect of the transfer surface conditions on the resulting normal and shear stresses was also studied; transfer surfaces made of machined steel (smooth) and transfer surfaces made of a bonded monolayer of glass particles (rough) were used. Although these transfer surfaces are radically different, the experiments did not show significant differences in normal stresses. The experimental results used in this study were collected using the same apparatus as used by Craig et al. [19]. As discussed in papers by Yu et al. [5] and Yu and Tichy [6], the present results are consistent with the those of the earlier Craig study.

### Background—Continuum Modeling

For steady flow of nearly elastic spherical granules of diameter  $D$ , density  $\rho_p$ , and mass  $m$ , the continuity equation can be written:

$$\rho = \frac{6m}{\pi D^3} v = \rho_p v \quad \rho \vec{\nabla} \cdot \vec{U} + \vec{U} \cdot \vec{\nabla} \rho = 0, \quad (1)$$

where mixture density  $\rho$ , and solid volume fraction  $v$ , are equivalent dependent variables. See various papers by Jenkins and co-workers for summaries of these types of continuum analyses (Jenkins and Richman [20] and Jenkins [21]). The mixture velocity is  $\vec{U}$ . The momentum equation is written in terms of the stress tensor  $\pi_{ij}$  (particle momentum flux in the  $i$ -direction through the  $j$ -surface due to the particle interactions):

$$\rho \frac{D}{Dt} \vec{U} = \rho \vec{g} - \vec{\nabla} \cdot \vec{\pi}. \quad (2)$$

Vectors are denoted by superscript arrows ( $\rightarrow$ ) and in later equations unit vectors are denoted by hats ( $\hat{\cdot}$ ). The double-ended arrow denotes a tensor quantity. The particle energy equation is (Johnson and Jackson [22] and Lun et al. [23])

$$\frac{3}{2} \rho \frac{D}{Dt} T = -\vec{\nabla} \cdot \vec{q} - \phi^f - \phi^c \quad \phi^f = \vec{\pi} : \vec{\nabla} \vec{U}, \quad (3)$$

where granular temperature  $T$  is defined as one third the square of the particles' velocity relative to that of the mixture. (A particle's instantaneous velocity is composed of both a mean and fluctuating component relative to the local flow velocity. Granular temperature uses only the fluctuating component). The  $\vec{q}$  is the molecular energy transport,  $\phi^f$  is the work rate of the momentum flux, and  $\phi^c$  is the inelastic work rate (dissipation) of the collisions. To differentiate from conventional temperature, which includes the effects of the mean velocity, granular temperature is sometimes called pseudo-temperature.

Equations (1)–(3) have essentially the same form as the corresponding classical fluid mechanics equations. The difference is in the constitutive equations or models relating the quantities. For example, classical materials obey Fourier's law of conduction:  $\vec{q} = -k \vec{\nabla} T$ , where  $k$  is the material property of conductivity, usually a constant. For the particulate system, the corresponding equation is often extremely complex. In the various theories (and they are numerous), the constitutive models are derived from assumptions of particle energy distributions, or from the simulations. A "property" such as conductivity depends on the local variables  $v$  and  $T$ , the boundary conditions of a particular problem, as well as other system and particle parameters such as coefficient of restitution, inter-particle friction coefficient, particle size distribution, etc. One cannot ascribe a conductivity or viscosity in the usual sense to such a mixture, e.g., a measurement of viscosity in one instrument has little or no predictive value in a different flow.

A model relating stress to the mixture velocity field is crucial to the continuum analysis. For a quasi-hydrodynamic incompressible material, the equation would be of the form

$$\vec{\pi} = p \vec{\delta} + \vec{\tau} \quad \vec{\tau} = -\eta(\dot{\gamma}) \vec{\dot{\gamma}} \quad \vec{\dot{\gamma}} = \vec{\nabla} \vec{U} + (\vec{\nabla} \vec{U})^T, \quad (4)$$

where  $\vec{\tau}$  is the extra stress determined from the motion,  $\eta$  is a non-Newtonian viscosity,  $p$  is pressure, and  $\vec{\delta}$  is the Kronecker delta. The symbol  $\vec{\dot{\gamma}}$  denotes the components of the rate-of-strain tensor. Such an equation would not suffice to properly describe the well-known experimental properties of granular shear flows. Regardless of what sort of viscosity function is used, this model predicts no load (normal stress) in Couette flow (simple shear between parallel plates), just as in conventional hydrodynamics. The load carrying stress  $\pi_{yy}$  equals  $p$ , since  $\tau_{yy} = \eta \gamma_{yy} = \eta \partial v / \partial y = 0$ . The pressure is found to be everywhere ambient along the film and thus does not contribute to load. A Reynolds equation derived from this equation will always say "no wedge or no squeezing means no load."

However, all existing experiments (e.g., Savage and Sayed [15], Yu et al. [5], and Hanes and Inman [24]) and particle simulations (e.g., Walton [17], Hopkins et al. [18], and Campbell and Brennan [13]) indicate that such normal load exists. An acceptable model may have a form like

$$\vec{\pi} = f_A(v, T) \vec{\delta} - f_B(v, T) \vec{\dot{\gamma}}. \quad (5)$$

The  $f$ 's are special constitutive relations. This equation predicts normal load carrying stress  $\pi_{yy} = f_A$ . Equations of this form are used by Khonsari in tribology studies (Dai et al. [9] and McKeeague and Khonsari [10]) and numerous others who are studying particle flows (Johnson and Jackson [22] and Lun et al. [23]).

Because properties such as solids fraction  $v$  vary across the gap, the momentum equation cannot be integrated, and thus a modified Reynolds equation cannot be obtained.

Another issue that distinguishes granular flows from hydrodynamic flows is the wall boundary condition. The situation is far more complex than to simply set the particle velocity equal to the wall sliding velocity. Proper boundary conditions are an active area of research and can lead to widely varying predictions, Jenkins and Richman [25] and Jenkins [26].

### Continuum Simulation of the Shear Cell

We treat the surface sliding speed  $U$ , the gap height  $H$ , and the unit normal load  $P_y$  as known input parameters. The dependent variables to be found are mixture velocity  $u$ , solids fraction  $v$ , and granular temperature  $T$ , all functions of cross-film coordinate  $y$ . For steady fully developed shear flow in a linear channel, such as (nearly) exists in experimental shear cells, the only velocity component is  $u(y)$ ; thus, the continuity equation is identically satisfied. In the absence of body force, the momentum equation components (2) become

$$0 = \frac{d\pi_{yx}}{dy} \quad (6a)$$

$$\pi_{yy} = \frac{F_y}{A} = P_y = \text{constant} \quad (6b)$$

The energy equation can be written as

$$0 = \frac{dq_y}{dy} + \phi^f + \phi^c. \quad (7)$$

Constitutive models for stress, conduction and dissipation have the following forms where the  $C$ 's are known complicated algebraic functions of solid fraction  $v$ , as well as particle density  $\rho_p$ , and coefficient of restitution  $e$ . We use some well-established formula due to Lun et al. [23], which we do not rewrite here due to space limitations.

$$\pi_{yx} = C_1[v(y)] \sqrt{T(y)} \frac{du(y)}{dy}, \quad (8a)$$

$$\pi_{yy} = C_2[v(y)] T(y) \quad (8b)$$

$$q_y = C_3[v(y)] \sqrt{T(y)} \frac{dT(y)}{dy} + C_4[v(y)] \sqrt{T^3(y)} \frac{dv(y)}{dy} \quad (9)$$

$$\phi^f = C_5[v(y)] \sqrt{T(y)} \left( \frac{du(y)}{dy} \right)^2, \quad (10a)$$

$$\phi^c = C_6[v(y)] \sqrt{T^3(y)} \quad (10b)$$

Equations (6)–(10) can be reduced to two ordinary differential equations. The temperature  $T = P_y / C_2$  can be eliminated using (6b) and (8b). Substituting  $T$  into (8a), then (8a) into (6a) gives

$$0 = \frac{d^2 u(y)}{dy^2} + B_1[v(y)] \frac{dv(y)}{dy} \frac{du(y)}{dy}, \quad (11)$$

where  $B_1 = 1/(C_1 \sqrt{P_y/C_2})(d/dv) C_1 \sqrt{P_y/C_2}$ . Substituting (9) and (10) into (7), and eliminating temperature yields

$$0 = \frac{d^2 v(y)}{dy^2} + B_2[v(y)] \left( \frac{dv(y)}{dy} \right)^2 + B_3[v(y)] + B_4[v(y)] \left( \frac{du(y)}{dy} \right)^2, \quad (12)$$

where the  $B$ 's are similar combinations of the  $C$ 's.

The boundary conditions are due to Jenkins and Richman [20]. There is a surface slip velocity of the particle mixture relative to the boundary wall. We have arranged the equations in terms of roughness factors for each term  $R$  ( $0 \leq R \leq 1$ , smooth:  $R=0$ , rough:  $R=1$ ). The Jenkins-Richman theory is developed

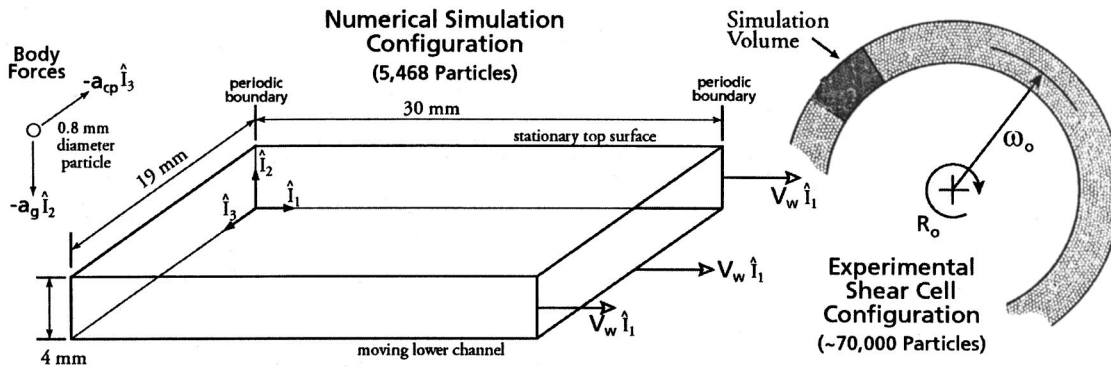


Fig. 2 Diagram of the simulation shear cell and the experimental shear cell configuration

for cylindrical disk particles of diameter  $D$ , with cylindrical disk wall roughness of diameter  $D_w$ . If the disk diameters and spacing  $\lambda$  are such that a particle fits exactly between the wall disks, there exists maximum roughness ( $R=1$ ). If the particle does not fit at all between the wall disks,  $R=0$ . The factors  $R_i B_i$  are complicated functions of  $D$ ,  $D_w$ , and  $\lambda$ ; but we simply treat the  $R$ 's as free parameters.

$$0 = \left( \pm \frac{du}{dy} + R_5 B_5 [v] u_{\text{slip}} \right)_{y=0,H} \quad (13)$$

$$0 = \left( \pm \frac{dv}{dy} + R_6 B_6 [v] v + R_7 B_7 [v] u_{\text{slip}}^2 \pm R_8 B_8 [v] u_{\text{slip}} \frac{du}{dy} \right)_{y=0,H} \quad (14)$$

$$u_{\text{slip}}|_{y=0} = U - u(0) \quad u_{\text{slip}}|_{y=H} = -u(H). \quad (15)$$

In Eq. (14), the energy flux at the wall balances the work rate due to the slip velocity and the inelastic work rate.

The governing Eqs. (11) and (12) are solved using a Runge-Kutta solver in *Mathematica*. A double loop process is used in which we guess  $v(0)=v(H)$  (outer loop) and  $u(0)=U-u(H)$  (inner loop) until the boundary conditions (13)–(15) are satisfied.

### Particle Dynamics Simulation of the Shear Cell

The molecular dynamics approach to multi-body problems has been widely used for a variety of different numerical studies. As applied to this problem—the annular shearing flow of identically sized glass spheres—the process has four main steps. The first step is to update each particle's position and velocity assuming that its travel is based on the physics of the simulation (gravitational body forces, etc.) and that the motion is independent of the overall particle configuration of the system. The next step is to check each particle to see if it is involved in a wall collision and, when required, use the appropriate boundary collision operator. The final step is to check each particle with each of its neighbors to see if they are occupying any of the same space. If they are, the appropriate collision operations are performed on this particle pair.

Because of the gross inefficiency of checking each particle with every other particle in the simulation (all pairs algorithm), researchers have devised a number of techniques to reduce the computational difficulty without compromising the physics of the simulation. In dense particle simulations neighbor lists are used. Particles that are close enough that they are likely to be involved

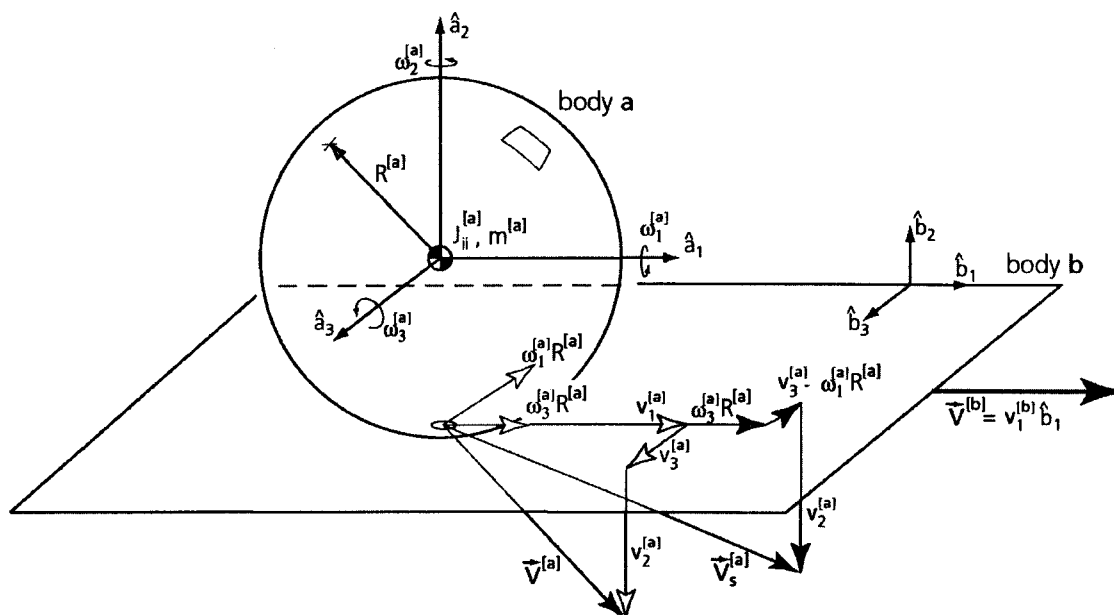


Fig. 3 Diagram of a representative collision between a particle and wall surface

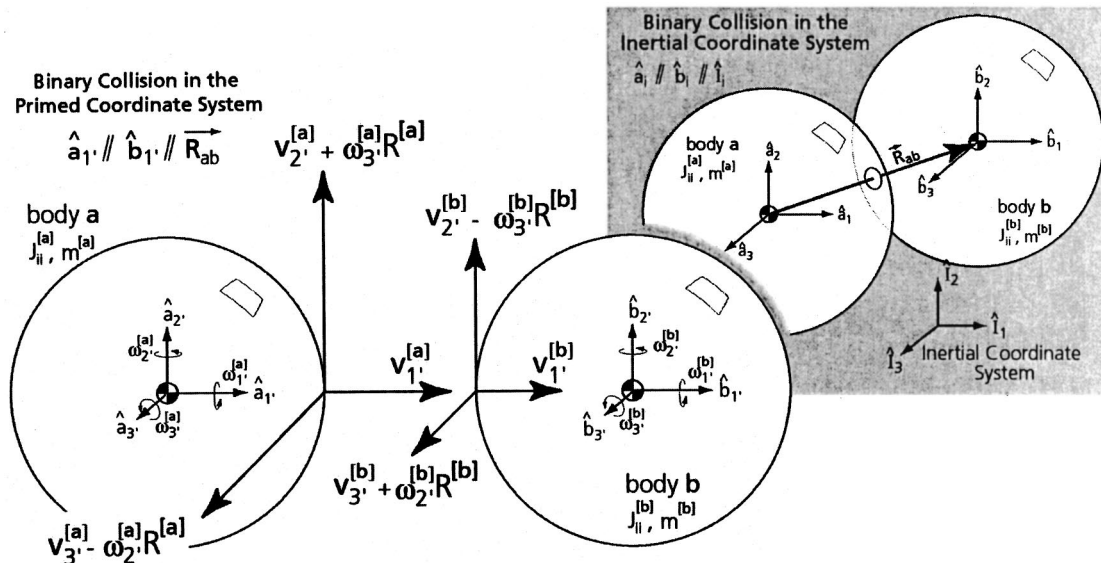


Fig. 4 Diagrams of a representative binary particle—particle collision. Inertial and body0-attached (primed) coordinate systems.

in a collision are kept in a list. The list must be periodically rebuilt as particles change their relative positions in the system configuration, Rappaport [27].

The particle dynamics applications are written in Java™, which is particularly useful for *n*-body simulations where the particles are data objects and the particle dynamics algorithms are container classes that operate on these data objects, Hudson et al. [28]. The event driven particle dynamics simulation assumes *a priori* that binary particle collisions are the dominant particle interactions and that the flow is a rapidly shearing granular flow.

The simulation shear cell configuration is designed to approximate our shear cell experimental apparatus and the granular collision lubrication experiments. The simulation shear cell is three-dimensional with periodic boundaries located across the flow and separated by a distance of  $L = 30$  mm, which represents approximately 7 percent of the entire shear cell circumference. The width and height of the shear cell trough correspond to experimental values. The simulation configuration is shown in Fig. 2.

**Body Forces.** The particle simulation includes two different body forces, gravity and centripetal acceleration to account for the cell rotation (however, body forces are not part of the continuum analysis). Gravitational acceleration acts in the negative  $\hat{i}_2$  direction and the centripetal acceleration acts in the negative  $\hat{i}_3$  direction. The inclusion of a centripetal body force warrants some dis-

ussion. In the absence of a carrier fluid, the particles travel ballistically between collisions. The particle's path of travel is independent of the shear cell configuration; the particle does not depend if it is in an annular shear cell, a cube, or a sphere. To account for the effects of the annular trough curvature on the particles relative position and velocity in the trough, a centripetal acceleration is imposed onto the particle ensemble. In this particular simulation cell, which is a Cartesian box, particles travel in a curved path accelerating towards the outer edge. In the "real" problem, particles travel in a straight line within a curved box. Unlike the gravitational body force, the centripetal accelerations are functions of both the particle's velocity and position within the annular trough.

**Particle Interactions with Smooth Frictional Walls.** The simulation walls are modeled as rigid smooth frictional surfaces. The top wall in the simulation is stationary while the bottom and sidewalls move at a constant speed. A collision between a particle and a bounding wall changes the particle's translational and angular velocity; the wall's velocity is unchanged. Rather than focusing on impulses arising from instantaneous impact, a time-averaged impulsive force for the collision is calculated by dividing the change in momentum by the simulation time step. The change in the particle's velocities (translational and angular) is a result of both normal and tangential forces acting between the particle and the wall. These forces are summed and used to calculate the normal and shear stresses acting on the wall surfaces, see Fig. 3.

The translational velocity, rotational velocity, and the tangential surface velocity at the contact point are given by Eqs. (16) and (17), respectively.

$$\vec{V}^{[a]} = v_1^{[a]}\hat{a}_1 + v_2^{[a]}\hat{a}_2 + v_3^{[a]}\hat{a}_3, \quad \vec{\omega}^{[a]} = \omega_1^{[a]}\hat{a}_1 + \omega_2^{[a]}\hat{a}_2 + \omega_3^{[a]}\hat{a}_3 \quad (16)$$

$$\vec{V}_s^{[a]} = (v_1^{[a]} + \omega_3^{[a]}R^{[a]})\hat{a}_1 + v_2^{[a]}\hat{a}_2 + (v_3^{[a]} - \omega_1^{[a]}R^{[a]})\hat{a}_3 \quad (17)$$

In this notation, the superscripts indicate a specific body while the vector component subscripts indicate a direction. The subscript *s* denotes particle surface velocity, as opposed to center of mass (no subscript). For particle contact with the lower sliding wall, the inertial system basis (unit) vectors  $\hat{i}_i$  line up with the body-

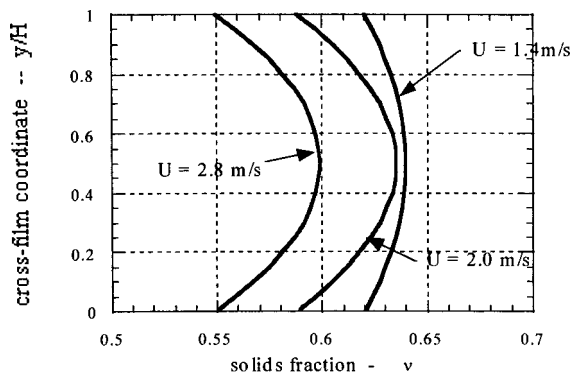


Fig. 5 Continuum model result. Variation of solid volume fraction across gap.

attached particle and wall basis vectors  $\hat{a}_i$  and  $\hat{b}_i$ . The resulting translational and angular velocity in the normal direction of particle  $[\mathbf{a}]$  after a wall collision are

$$v_2^{[a]}|_{t=\Delta t} = -v_2^{[a]}|_{t=0} e^{[ab]} \quad \omega_2^{[a]}|_{t=\Delta t} = \omega_2^{[a]}|_{t=0}. \quad (18)$$

The average contact force between body  $[\mathbf{a}]$  and the wall surface  $[\mathbf{b}]$  during a collision can be found by dividing the magnitude of the momentum change of body  $[\mathbf{a}]$  by the duration of time over which the exchange occurs. It is convenient to use one simulation time step  $\Delta t$  for these types of time averages.

$$\bar{F}_n^{[ab]} = \frac{m^{[a]}|v_2^{[a]}|(1 + e^{[ab]})}{\Delta t} \hat{a}_2 \quad (19)$$

$$\begin{aligned} \bar{F}_f^{[a]} = \mu^{[ab]} |\bar{F}_n^{[ab]}| & (\text{sgn}(v_1^{[b]} - (v_1^{[a]} + \omega_3^{[a]} R^{[a]})) \hat{a}_1 \\ & + \text{sgn}(v_3^{[b]} - (v_3^{[a]} - \omega_1^{[a]} R^{[a]})) \hat{a}_3). \end{aligned} \quad (20)$$

Equation (19) is the average normal force that acts on body  $[\mathbf{a}]$  as a result of a wall collision while Eq. (20) is the frictional or tangential force. The normal and friction forces that act on the wall surface, body  $[\mathbf{b}]$ , are equal in magnitude and opposite in direction of those forces acting on body  $[\mathbf{a}]$ . The quantity  $v_1^{[b]} - (v_1^{[a]} + \omega_3^{[a]} R^{[a]})$  is the surface slip velocities in the  $\mathbf{1}$ -direction between bodies  $[\mathbf{a}]$  and  $[\mathbf{b}]$ . During a collision, bodies are able to apply frictional forces to each other until the point of pure rolling (zero slip) is reached.

Equivalent forces and moments on the particle center of mass as a result of the surface traction force vector, Eqs. (19) and (20) are also found. Assuming that the average surface traction force is constant over some currently unknown incremental time  $\Delta \tau_1$ , a particle's translational and rotational velocities are given as

$$\begin{aligned} v_1^{[a]}|_{t=\Delta \tau_1} &= v_1^{[a]}|_{t=0} + \frac{f_1^{[a]}}{m^{[a]}} \Delta \tau_1, \\ \omega_3^{[a]}|_{t=\Delta \tau_1} &= \omega_3^{[a]}|_{t=0} + \frac{M_3^{[a]}}{J_{33}^{[a]}} \Delta \tau_1. \end{aligned} \quad (21)$$

The surface sliding velocity component in the  $\mathbf{1}$ -direction after the elapsed times  $\Delta \tau_1$  is

$$v_{s_1}^{[a]} = v_1^{[a]} + \frac{f_1^{[a]}}{m^{[a]}} \Delta \tau_1 + \omega_3^{[a]} R^{[a]} + \frac{M_3^{[a]}}{J_{33}^{[a]}} R^{[a]} \Delta \tau_1. \quad (22)$$

The symbol  $J_{33}^{[a]}$  is the polar moment of inertia of the sphere about the  $\mathbf{3}$ -direction of particle  $[\mathbf{a}]$ . The amount of time needed to eliminate sliding in the contact in the  $\mathbf{1}$ -direction can then be found by setting the surface velocities to zero and for  $\Delta \tau_1$ :

$$\Delta \tau_1 = \frac{v_{s_1}^{[a]} - (v_1^{[a]} + \omega_3^{[a]} R^{[a]})}{\frac{f_1^{[a]}}{m^{[a]}} + \frac{M_3^{[a]}}{J_{33}^{[a]}} R^{[a]}} \quad (23)$$

To save space, only one of the two component equations is shown.

If the time needed to eliminate slip in the contact  $\Delta \tau_i$  is greater than the simulation time step  $\Delta t$  then  $\Delta \tau_i$  is set equal to the simulation time step and Eq. (21) is used to update the particle's velocity. This is physically reasonable because the simulation time step is the time increment used for the momentum exchange, Eq. (19), to obtain the average contact force during the collision. If the time needed to eliminate slip in the contact  $\Delta \tau_i$  is less than the simulation time step  $\Delta t$ , then  $\Delta \tau_i$  is left as is. Again, Eq. (21) is used to update the particle's velocity.

**Binary Particle Collisions.** Details are similar to the wall-particle case so we only provide a few comments. The particles are modeled as rigid smooth frictional spheres. Similar to a colli-

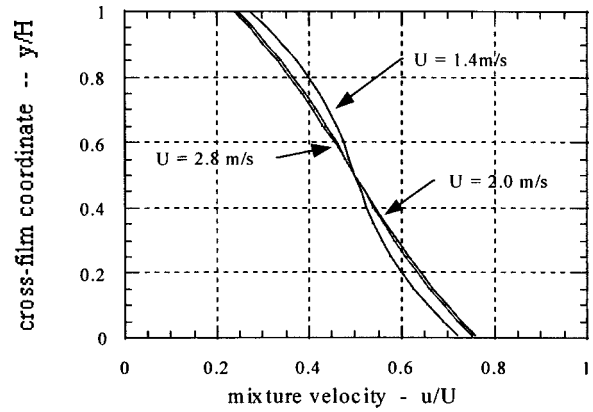


Fig. 6 Continuum model result. Variation of mixture velocity across gap.

sion between a particle and a container surface, the particle/particle collision is three-dimensional and includes the effects of translational velocity, angular velocity, as well as the particle's mass and radius. The coefficient of friction, and the coefficient of restitution for the collision are also imposed. The particle collision algorithm also makes use of body-attached coordinate systems, and transforms the three-dimensional collision into a much simpler, but equivalent, one-dimensional collision where the approach-of-centers vector is parallel to the  $\mathbf{1}'$  axis, see Fig. 4.

As in the wall-particle case, the program solves for the time to eliminate slip in the contact  $\Delta \tau_i$ . If this time is less than the simulation time step  $\Delta t$ , then it is used as the time over which the forces act. The time over which the traction forces act is then used to find the post collision velocities.

## Results

**Continuum Model.** The input parameters are  $D=0.787$  mm, density  $\rho_p=2550$  kg/m<sup>3</sup>,  $H=4$  mm, as reported above for the experiment. The input linear sliding speeds used are  $U=1.4, 2.0$  and  $2.8$  m/s; and input applied normal loads used are  $P_y=2.5, 5.0,$  and  $10.0$  kPa. Other parameters needed can only be crudely estimated: for the surface roughness parameter (both surfaces) we set  $R_5=R_6=R_7=R_8=0.5$ , and for the coefficient of restitution of the particle and the wall  $e_p=0.9$  and  $e_w=0.9$ , respectively. The wall coefficient  $e_w$  is needed for the functions  $B_5$ – $B_8$ , see Eqs. (13)–(14).

For the case  $P_y=5.5$  kPa, the variation of solid fraction across the film is shown in Fig. 5 for  $U=1.4, 2.0,$  and  $2.8$  m/s. The mean solid fraction  $\bar{v}$  for the three cases is  $0.63, 0.58,$  and  $0.51$ , respectively. For higher loads, the mean solid fraction is higher and the variation across the film is smaller—the particles are densely packed almost to the maximum. For the same three cases, the normalized velocity profiles are shown in Fig. 6. A slight deviation from the linear Couette flow is exhibited and the slip velocities are nearly identical. At higher loads the velocity distribution is more linear. At much smaller loads ( $P_y \sim 0.1$  kPa, not shown) the slip effect at the boundary is greatly exaggerated and nearly slug flow is seen away from the walls.

**Particle Simulations.** A program summary of a simulation is shown in Fig. 7. Note in Fig. 8, that the particles generally tend to stay in place, particularly, packed toward the lower left side due to the gravity and centripetal body forces.

Normal stresses are calculated from

$$\pi_{22} = \frac{1}{(\text{area}) \Delta t} \sum_{j=1}^{N_t} m^{[j]} v_2 (1 + e^{\text{wall}}), \quad (24)$$

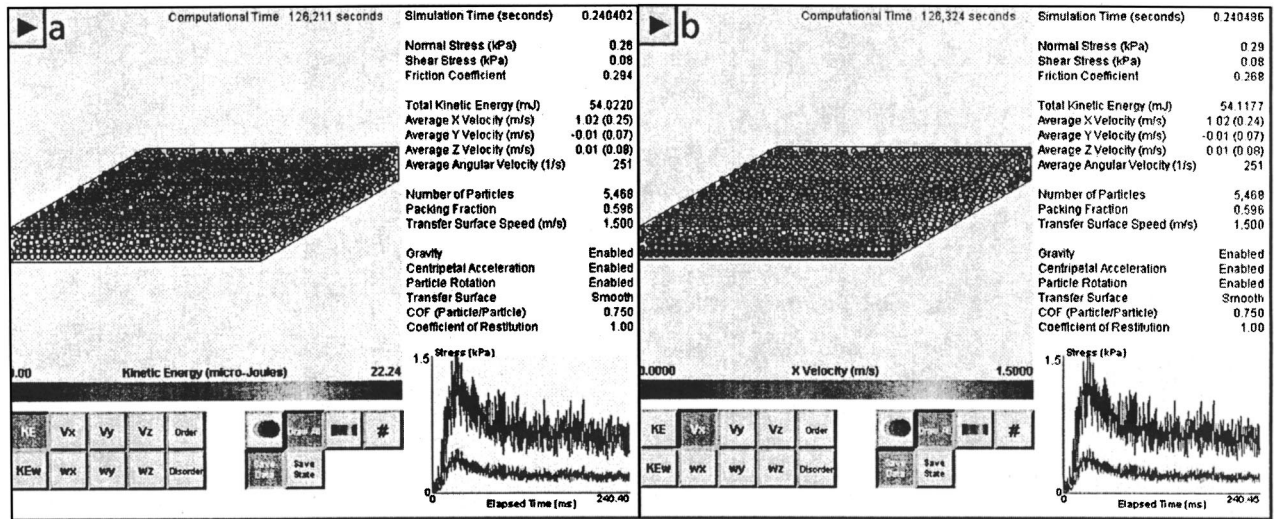


Fig. 7 A particle dynamics simulation. Contour plots of the same configuration at specific instants in time: (a) the particle's translational kinetic energy; (b) the particle's flow direction velocity.

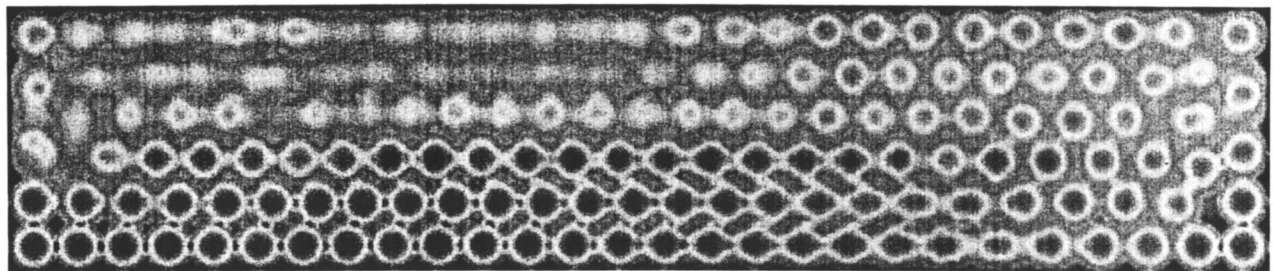


Fig. 8 Density contour plot of the simulation volume; flow direction is out of the page.

where the  $j$  refers to the number of wall collisions in the given time step and area is the surface area.

**Comparison to Experiment.** Normal stress data for the continuum and particle dynamics models are compared to experimental results in Fig. 9, and global shear force in Fig. 10. The standard deviation error bars shown are for simulation stresses that are time averaged over a duration of 0.05 ms or 100 simulation time steps.

The trends and orders-of-magnitude are in agreement. The log-log slope in all cases (both theories and experiment) is nearly two, implying that we are operating in the collision mode, the forces being generated by kinetic energy, proportional to velocity squared. The fact that the particle simulation and the continuum model are in near perfect agreement for the normal stress case must be ascribed to good fortune. The particle simulations and the continuum model are in reasonable agreement with the experi-

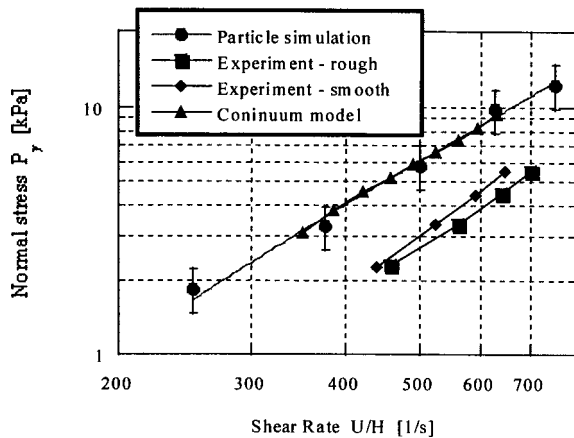


Fig. 9 Normal load behavior: comparison of continuum and particle dynamics analysis to experiment.

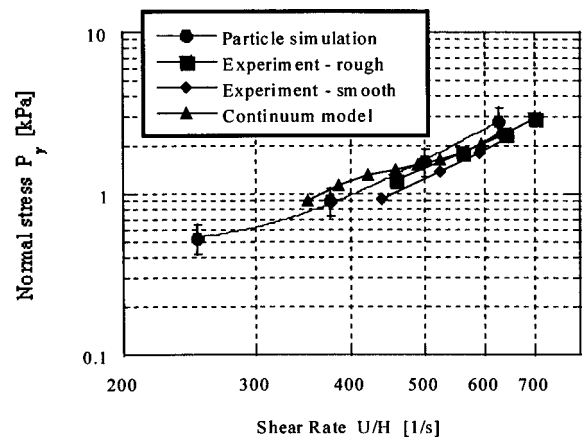


Fig. 10 Shear force behavior: comparison of continuum and particle dynamics analysis to experiment.

mental measurements of shear stress. However, both the particle simulations and the continuum model significantly over-predict the experimental measurements of normal stress.

## Conclusions

At first blush the agreement of the two theoretical predictions with the experiment and with each other is not particularly impressive. However, note that the particle simulation and continuum modeling are both determined completely by first principles. There has been no curve fitting or basing the results on species determinations of viscosity or other implied properties of the mixture. Furthermore, we did no adjustment of the unknown parameter values (friction coefficient between the particles, coefficient of restitution, or surface roughness coefficient) to obtain a better fit, which could certainly be done; rather we simply stayed with our original best guess. There are many available models for the  $C$  functions of Eqs. (8)–(10) and slip boundary conditions (13)–(15) and we did not experiment for a better fit. As an initial point of departure toward developing a high level of predictive ability, we are pleased with the agreement. The particle simulation can also serve as a means to develop simpler more usable continuum approaches.

The present results would seem to shed some light on an issue concerning the effect of the centrifugal body force on the particles due to the curvature of the shear cell. Researchers have speculated that centrifugal force would pack the particles to the outside wall and suppress the collision regime. Such packing does occur, but the particles remain surprisingly ordered and densely packed all across the channel so the effect of the centrifugal force seems to be small. In fact, the surprising conclusion is that the particle flow is so significantly ordered while the global result is that we are operating in the granular collision mode, which at least conceptually draws many parallels to the disordered behaviors of gases.

As discussed in the literature survey, advanced particle simulation programs with a rheology and mechanics focus do exist. Ours is by far the most advanced to address particle flow with a tribology perspective. To our knowledge, the only simulation competitor in the tribology field is a two-dimensional (rigid disks) two-degree of freedom (no rotation) simulation due to Elrod [29] compared to our full three-dimensional, 6 DOF capability.

## References

- [1] Ali, I., Roy, S. R., and Shin, G., 1994, "Chemical-Mechanical Polishing of Interlayer Dielectric: A Review," *Solid State Technol.*, pp. 63–69.
- [2] Tichy, J. A., Levert, J. A., Shen, L., and Danyluk, S., 1999, "Contact Mechanics and Lubrication Hydrodynamics of Chemical-Mechanical Polishing," *J. Electrochem. Soc.*, **146**, pp. 1–7.
- [3] Cho, U., and Tichy, J. A., 1997, "Quantitative Correlation of Wear Debris Analysis," *World Tribology Congress*, Institute of Mechanical Engineers.
- [4] Poggie, R. A., Mishra, A. K., and Davison, J. A., 1994, "Three-Body Abrasive Wear Behavior of Orthopedic Implant Bearing Surfaces from Titanium Debris," *J. Mater. Sci.: Mater. Med.*, **5**, pp. 387–392.
- [5] Yu, C. M., Craig, K., and Tichy, J. A., 1994, "Granular Collision Lubrication," *J. Rheol.*, **38**, pp. 921–936.
- [6] Yu, C. M., and Tichy, J. A., 1996, "Granular Collision Lubrication: Effect of Surface Roughness, Particle Size Solid Fraction," *STLE Tribol. Trans.*, **39**, pp. 537–546.
- [7] Heshmat, H., 1991, "High-Temperature Solid-Lubricated Bearing Development-Dry Powder-Lubricated Traction Testing," *AIAA Journal of Propulsion and Power*, **75**, pp. 814–820.
- [8] Heshmat, H., 1992, "The Quasi-Hydrodynamic Mechanism of Powder Lubrication: Part 2. Lubricant Film Pressure Profile," *Lubr. Eng.*, **48**, pp. 373–383.
- [9] Dai, F., Khonsari, M. M., and Lu, Y. Z., 1994, "On the Lubrication Mechanism of Grain Flows," *STLE Tribol. Trans.*, **37**, pp. 516–524.
- [10] McKeague, K. T., and Khonsari, M. M., 1995, "Generalized Boundary Interactions for Powder Lubricated Couette Flow," *ASME J. Tribol.*, **117**, pp. 1–8.
- [11] Campbell, C., and Zhang, Y., 1991, "The Interface between Fluid-Like and Solid-Like Behavior in Granular Flows," *Advances in Micromechanics of Granular Materials, Studies in Applied Mechanics*, H. Shen et al., Eds., **31**, pp. 261–270.
- [12] Savage, S. B., 1998, "Analyses of Slow High Concentration Flow of Granular Materials," *J. Fluid Mech.*, **177**, pp. 1–26.
- [13] Campbell, C. S., and Brennen, C. S., 1985, "Computer Simulations of Granular Shear Flows," *J. Fluid Mech.*, **151**, pp. 167–188.
- [14] Bagnold, R., 1954, "Experiments on a Gravity-Free Dispersion of Large Solid Spheres in a Newtonian Fluid under Shear," *Proc. R. Soc. London, Ser. A* **225**, pp. 45–63.
- [15] Savage, S. B., and Sayed, M., 1984, "Stresses Developed by Cohesionless Granular Materials Sheared in an Annular Shear Cell," *J. Fluid Mech.*, **142**, pp. 391–430.
- [16] Walton, O., and Braun, R., 1993, "Simulation of Rotary-Drum and Repose Tests for Frictional Spheres and Rigid Sphere Clusters," *Joint DOE/NSF Workshop On Flow of Particulates and Fluids*, Ithaca, NY.
- [17] Walton, O., 1993, "Numerical Simulation of Inelastic Frictional Particle-Particle Interactions," *Particulate Two-Phase Flow*, M. Roco, Ed., chap. 25, Butterworth-Heinemann, Boston, MA.
- [18] Hopkins, M., Jenkins, J., and Louge, M., 1991, "On the Structure of 3D Shear Flows," *Advances in Micromechanics of Granular Materials, Studies in Applied Mechanics*, H. Shen et al., Eds., **31**, pp. 271–279.
- [19] Craig, K., Buckholz, R., and Domoto, G., 1986, "An Experimental Study of the Rapid Flow of Dry Cohesionless Metal Powders," *ASME J. Appl. Mech.*, **53**, pp. 935–942.
- [20] Jenkins, J., and Richman, M. W., 1985, "Kinetic Theory for Plane Flows of a Dense Gas of Identical, Rough, Inelastic, Circular Disks," *Phys. Fluids*, **28**, pp. 3485–3495.
- [21] Jenkins, J., 1987, "Rapid Flows of Granular Materials," in *Non-Classical Continuum Mechanics*, Cambridge Press, Cambridge, United Kingdom, pp. 213–225.
- [22] Johnson, P. C., and Jackson, R., 1987, "Frictional-Collisional Constitutive Relations for Granular Materials with Applications to Plane Shearing," *J. Fluid Mech.*, **176**, pp. 67–93.
- [23] Lun, C. K. K., Savage, S. B., Jeffrey, D. J., and Chepurnyi, N., 1984, "Kinetic Theories for Granular Flows: Inelastic Particles in Couette Flow and Slightly Inelastic Particles in a General Flow Field," *J. Fluid Mech.*, **140**, pp. 223–256.
- [24] Hanes, D. M., and Inman, D. L., 1985, "Observations of Rapidly Flowing Granular Fluid Materials," *J. Fluid Mech.*, **150**, pp. 357–380.
- [25] Jenkins, J. T., and Richman, M. W., 1987, "Boundary Conditions for Plane Flows of Smooth, Nearly Elastic, Circular Disks," *J. Fluid Mech.*, **171**, pp. 53–69.
- [26] Jenkins, J., 1990, "Boundary Conditions for Rapid Granular Flows: Flat, Frictional Walls," *ASME J. Appl. Mech.*, **59**, pp. 120–127.
- [27] Rappaport, D., 1997, *The Art of Molecular Dynamics Simulation*, Cambridge University Press, Cambridge, United Kingdom.
- [28] Hudson, J. B., Sawyer, W. G., Bryson, D., and Svanes, T., 1997, "An Interactive Molecular Dynamics Simulation of Atomic Behavior," *National Educators Workshop Conference Proceedings*, Seattle, WA.
- [29] Elrod, H., 1996, "Numerical Experiments with Flows of Elongated Granules," *Tribology Series 31, Proceedings of 22nd Leeds-Lyon Symposium*, Elsevier, Amsterdam, pp. 347–354.